Vehicle sensing in optically and thermally obscured environments

Ee Kent Lew, Benjamin Shih

Electrical and Computer Engineering, Carnegie Mellon University

***Abstract*— This report presents a magnetometer designed to detect vehicles in optically and thermally obscured environments. Due to the ferromagnetic properties of materials used in the construction of vehicles, vehicles perturb the Earth's magnetic field. The magnetometer senses these perturbations through electromagnetic induction. Signal processing techniques are employed to harness and amplify actual signal from environmental noise. The design, layout, physics, principles of operation, performance characteristics and limitations are theoretically and experimentally discussed in this paper. It is found that the transfer characteristics are extremely non-linear and the device is limited by Johnson noise.**

***Index Terms*— magnetism, magnetic field perturbation, magnetic flux, vehicle detection, non-line-of-sight sensing, remote sensing, electro-magnetic induction.**

I. INTRODUCTION

Current vehicle sensors today are heavily limited by sensing range. Most vehicle sensors employ the induction loop method for detecting vehicles, and are primarily used in highway and parking systems. These induction loop sensors are buried underground and positioned 1-2 feet away from the vehicle base. Their sensing range and direction are heavily limited due to their magnetic energy and physical size constraints. Increasing their range would lead to significantly impractical increases in power consumption, radiated magnetic energy and physical size.

Longer range vehicle sensors employed by commercial and military users include radar, Light Detection and Ranging (LIDAR), infra-red, ultrasound, EM-signal triangulation such as GPS and radio-tower triangulation. The effectiveness of these techniques is reduced in optically and thermally obscured environments.

This paper presents a magnetometer that is designed and calibrated for remote sensing of vehicles with a range that exceeds current inductive loop sensors in the market; physical dimensions that are significantly smaller than existing sensors; higher mobility and the potential to scale up towards 3-dimensional sensing. The sensor system proposed is capable of sensing vehicles in optically and thermally obscured environments such as sandstorms by detecting changes in the Earth's magnetic field. These fluctuations are not susceptible to environmental conditions.

Applications of the sensor system include commercial applications for vehicle detection in highways and parking systems, and vehicle safety in collision detection systems. Military applications include the detection of military vehicles and equipment for defensive force protection; early warning and remote sensing capabilities; and vehicle detection for pyrotechnics such as mines, intelligent and guided munitions.

II. DESCRIPTION OF PHYSICS

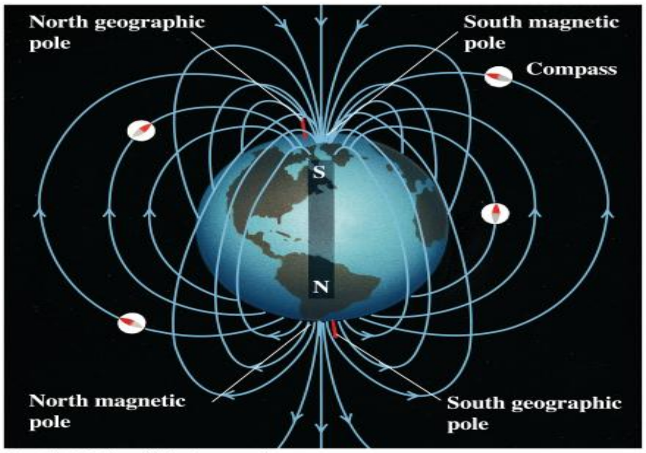

Fig. 1. Visualization of the Earth's magnetic field

The magnetic field strength on the Earth's surface varies from 0.25 to 0.65 Gauss, or 25000 to 65000 nT (National Geophysical Data Center). For the purpose of our sensor system to be used in North America, we can accurately estimate that the Earth's magnetic field strength on the surface of North America is 0.55 Gauss (U.S. Geological Survey). To operate the sensor in other areas, the sensor can be calibrated against a different environment's magnetic field strength.

Fig. 2 shows a matlab visualization of how a standard size vehicle perturbs the Earth's surface magnetic field. The red centered sphere represents a standard vehicle. Earth's magnetic field travels from top to bottom. We can see that the field converges into the car and diverges out of the car, leaving a region of magnetic vacuum surrounding the car perpendicular to the field direction.

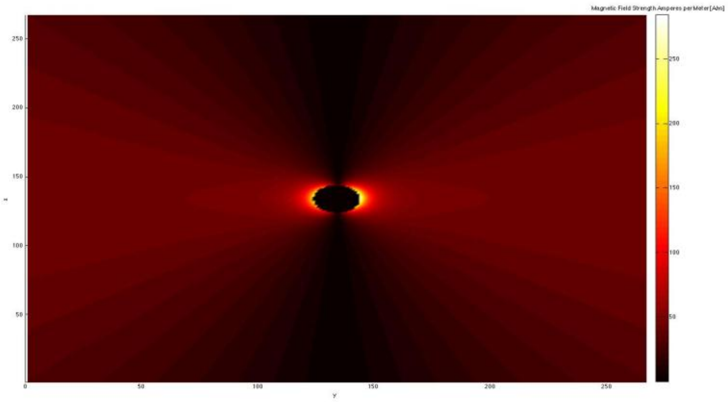

Fig. 2. Matlab visualization of a vehicle's distortion of the Earth's magnetic field

In the diagram above, the Earth's magnetic field travels from the right to left. Through modelling, it is found that perturbations of the Earth's magnetic field by the vehicle (black sphere centered in the picture) as a function of distance can be characterised by the following relationship:

$$\Delta H = 2 \cdot 43.69 \cdot \cos(\Theta) \cdot \left[\frac{Ur - 1}{Ur + 2} \cdot \left(\frac{R}{r}\right)^{3} + \frac{1}{2} \right] \qquad (1)$$

R is defined to be the radius of sphere centered onto Fig.2 and simulates an ordinary standard-sized passenger vehicle. 'r' is defined as the separating distance between the vehicle and the magnetometer sensor. μr is the relative permeability of the material in the vehicle. For the purposes of our simulation, we chose a value of 100 as an accurate approximation with metals used for the construction of vehicles. The angle phi is defined to be the angle of deviation of the sensor with respect to the vehicle with the reference point at parallel to the Earth's background magnetic field direction.

Our choice of material for our magnetometer is the N30 ferrite core consisting of base material MnZn. This material gives us the following B-H curve shown in Fig. 3. An approximation of the curve using power series was obtained and illustrated by the black curve with its equation.

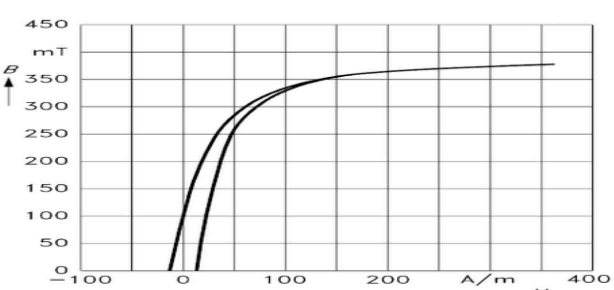

Fig. 3. Approximation of B-H curve.

From Fig. 3 above, the core saturates when the H field exceeds 100 amperes per meter (A/m). The desired region of operation for the sensor is non-saturation, where the H-field will never exceed 100A/m. For this region of operation, the power series expansion is:

$$y = 3E\text{-}05x^3 - 0.0226x^2 + 5.2491x \qquad (2)$$

The model is accurate for characterizing the B-H characteristic of our choice of material. Equation 2 will be the quantitative model our magnetometer will be based upon. The region of operation for the sensor is when H-field is between x and y.

III. SENSOR STRUCTURE AND PRINCIPLES

Fig. 4 shows the system-level setup of our sensor system with the various circuit components.

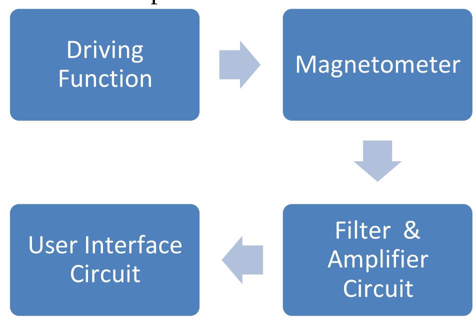

Fig. 4. Flow chart for sensor system.

The proposed Function Generating Circuit (FGC) has the following circuit schematic as shown in Fig. 5:

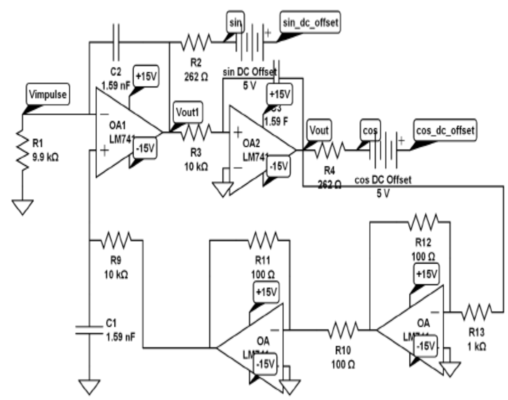

Fig. 5. Function generating circuit used to produce sine wave.

The function generating circuit is modeled after a quadrature oscillator, and produces 1kHz sine and cosine waves, both with a 5V DC offset. The circuit consists of two primary Op-amps (OA1, OA2), which are integrators. Each individual output is fed into the input of the other Op-amp, and the only pair of functions which can be integrated repeatedly and retain the same oscillation is sine and cosine. The second stage consists of an inverting amplification stage with gain 10, as well as a unity gain inverting amplifier that acts as a buffer for the sign of the signal in order to obtain a more easily detectable driving function. A switch is used at V-impulse to initialize the feedback oscillations necessary to produce the sine and cosine outputs waveforms. This gives the option of mobility to the sensor system for field tests in different environments. For the purposes of our project, testing was conducted in the laboratory using the Agilent Function Generator in place of the function generating circuit.

The function generator produces a sine wave signal with amplitude of 10 volt at a frequency of 1KHz with 5 voltage offset. This signal will be fed into the Driving Excitation Coil (DEC) on the left of the magnetometer shown in Fig. 6:

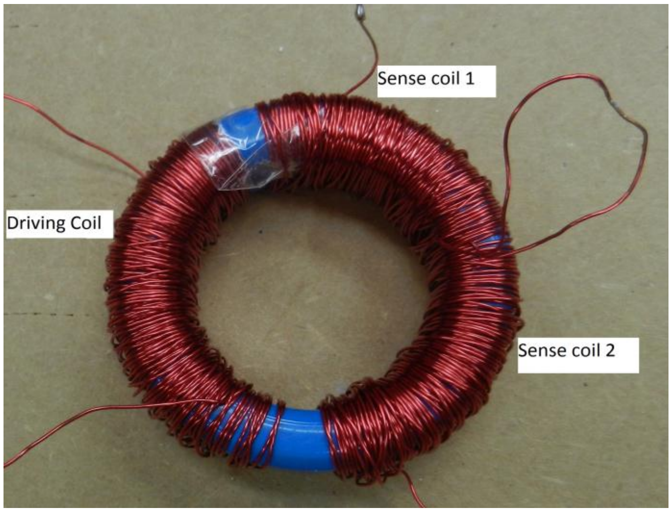

Fig. 6. Magnetometer core compared to a dollar coin.

The dimensions of the magnetometer core (blue) are: outer diameter = 58.3 mm, inner diameter = 40.8 mm, height = 17.6 mm, impedance of the driving coil = 843 ohms. The DEC has 150 turns wound tightly in two layers. The magnetic field (H) produced by the excitation coil can be characterized by the following equation:

$$Ho = \frac{Idec * Ndec}{le} \tag{3}$$

On the left of the magnetometer core are two Sensing Detector Coils (SDC): SDC 1 (top coil) and SDC 2 (bottom coil). SDC 1 and 2 are wound tightly in layers around the core and in opposite directions, such that the electromotive force (EMF) induced in one coil cancels out that of the other coil. The magnetometer sensor measures changes in the background magnetic field strength through variations in the induced EMF at the sense coils.

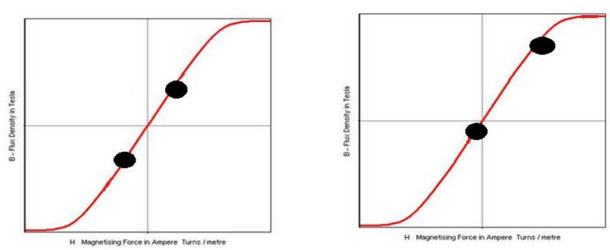

Figure 7: B-H Curve operating points for sensing coil 1 (Left) and 2 (Right) without voltage offset.

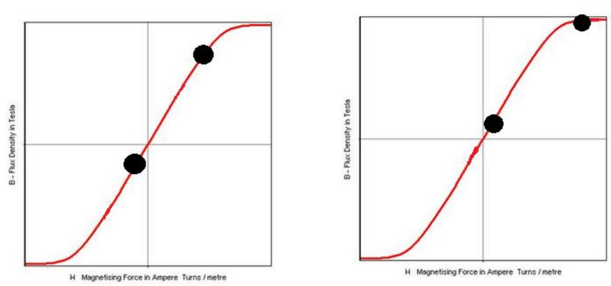

Figure 8: B-H Curve operating points for sensing coil 2 (Left) and B (Right) with voltage offset.

Given an arbitrary input function from the driving coil with a total peak-to-peak spanning the black markers in Fig. 7 and Fig. 8, the location on the B-H curve of the core with an unperturbed magnetic field varies with and without an offset applied to the driving function. Assuming sense coil 1 is parallel and sense coil 2 is perpendicular to the Earth's magnetic field. Without applying an offset to the B-H curve of the ferromagnetic core, the operating point of the core is depicted in Fig. 7. Assuming no magnetic field detection in coil 2, and given some input, the resulting output peak-to-peak spans some range on the B-H curve. Now, given the same input, but in coil 1, the output span on the B-H curve will simply be shifted while remaining in a linear region. In this regime, the output will shift the same amount as the input whether or not the sensing coils are affected by a background magnetic field strength. Thus, in terms of differences in the B-H curve magnitude, no change in magnetic flux, and thus no object, can be detected. Since both sensing coils are wound oppositely, the change in magnetic flux in both coils is exactly the same due to its linear operating point, despite the operating point being shifted. On the other hand, Fig. 8 denotes the desired operating point on the B-H curve that will enter the magnetic saturation region when the driving function has a voltage DC offset. In this situation, given some input, the offset combined with coil 1 will result in a non-linear relationship between the input and output, whereas the region of coil 2 will remain in a linear operating regime. The saturation of the ferromagnetic core's B-H curve causes the resulting difference in the output signal of the device. By operating on the B-H curve with an offset, the device can be used to detect disturbances in the Earth's magnetic field.

Each SDC will have an end probe, and they will be connected to the Signal Amplifying Circuit in Fig. 9 to boost the amplitude of our signal.

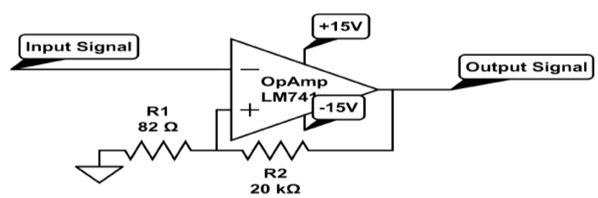

Fig. 9. Signal Amplifying Circuit.

IV. USER INTERFACE CIRCUIT

For our laboratory demonstration we build an envelope detector circuit for analysis. The envelope detector in Fig. 10 is connected after the amplifier circuit to trace the peak values of the alternating signal.

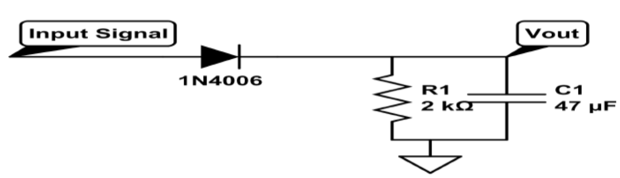

Figure 10: Envelope Detector Circuit

Alternatively, for future work we propose using an Analog-to-Digital converter with a sampling frequency (2.1KHz), just over twice that of the input signal (1 KHz) in accordance to the Shannon-Nyquist sampling theorem. The output voltage from the Signal Amplifier Circuit will be fed into a 16-bit Analog-to-Digital converter. The ADC has an operating temperature range of 0 to 70 degrees Celsius with a Signal-to-Noise Ratio (SNR) of 90 dB at 1 KHz. Its input ranges from -12 to 12 volts and has an input impedance of 7.9 Ohms. Its acquisition time is 1.82 microseconds, which is more than sufficient for our sampling frequency. The output from the 16 bit ADC will enable recording and further analysis currently outside the scope of this sensor project. The output from the ADC will also be channeled into a RMS-to-DC converter AD637 which will compute the true RMS value of the Vout sinusoidal waveform. The AD637 has an operating temperature of 0 to 70 degrees Celsius and a bandwidth of 9MHz for the input its voltages.

V. TESTING

For the purposes of testing and characterizing our sensor system, we used an air-core solenoid with a radius of 17mm and 565 turns of magnetic wire. The current through the wire coil is 0.55 amperes at 3.12 volts. This creates a turn density of 194 turns/cm. The device produces a field of:

$$B\ (Magnetic\ Field) = 4 * \pi * e^{-7} * 194 * 0.55$$
$$= 0.000135\ Tesla$$
$$= 1.35\ Gauss$$

We used this solenoid to simulate the vehicle of interest, and characterized our sensor system with this test solenoid device. Out final data of interest is the output voltage obtained from the envelope detector. We obtained the transfer function of:

$$V(Out) = 0.0108r^4 - 0.33r^3 + 3.7244r^2 - 18.868r + 40.334 \quad (4)$$

'r' is the distance between the sensor and solenoid.

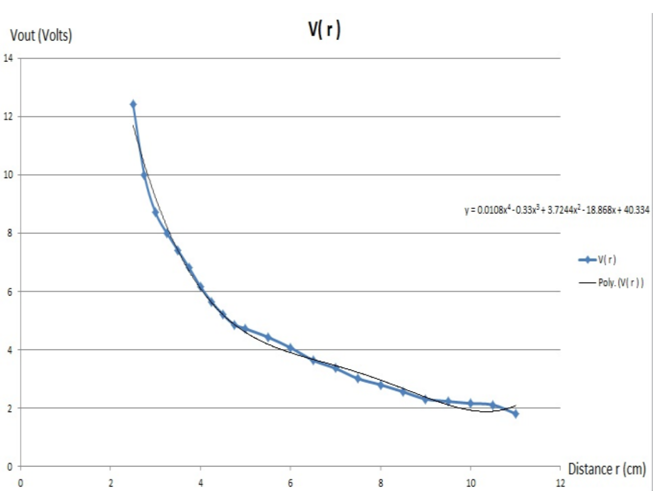

Figure 11: Transfer function

VI. SENSOR CHARACTERISTICS

A. *Calculated Sensitivity*

$$\text{Sensitivity} = dVout/dr$$
$$\text{Sensitivity} = 0.0432r^3 - 0.99r^2 + 7.4488r - 18.868$$

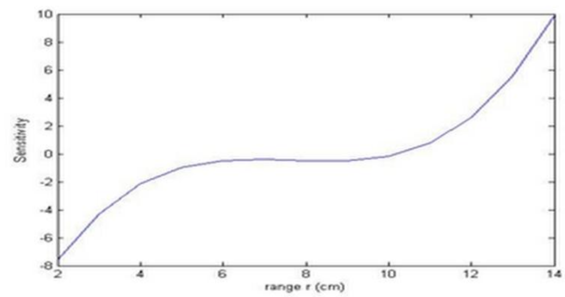

Fig. 12. Plot of sensitivity vs. distance from perturbation.

We note that sensitivity is non-linear and decreases as distance ranges from 2.5cm to 6cm, and stays fairly constant from 6cm to 10cm. It increases from 10cm thereafter which is caused by the non-ideal approximation of our transfer function with a fourth order polynomial estimate.

B. *Linearity:*

Although the transfer function is inherently non-linear, other sources also contribute to the non-linearity of the sensor system. These external sources include:

1. Wire diameter variations in the driving and sensing coils.
2. Non-uniformity of wire windings.
3. Changing of resistance in wires with variations of temperature.

C. *Dynamic range*

i. *Span*

The maximum sensing distance (r) of our sensor is determined by the sensitivity of our sensor. At further distances, our sensitivity decreases. Through experimentation, our maximum reasonable sensing range is 11cm at 1.81 volts. The nearest distance our sensor can operate is at the surface of the vehicle is 2.5cm at 12.4 volts. This is because our amplifier goes into saturation of 12.5 volts for distances nearer than 2.5 cm.

ii. *Dynamic Range*

The dynamic range is calculated as the log of the ratio of the range. The minimum incremental resolution of our sensor is 0.05V.

$$20*\log_{10}((12.4-1.81)/0.05V) = 46.5\ dB$$

iii. *Resolution*

The resolution of the sensor is given by:

$$Res = \frac{(Voltage\_Span)(Distance\_Res)}{Distance\_Span} = \frac{(12.4-1.81)(0.25cm)}{8.5cm} = 0.311V$$

Resolution is limited by potential sources of interference and the Signal-to-Noise Ratio (SNR) of the electrical components used in the sensor system.

D. *Hysteresis*

Magnetic hysteresis is an issue if the toroid core is brought to saturation levels. Fig.13 below shows the graphical representation of hysteresis:

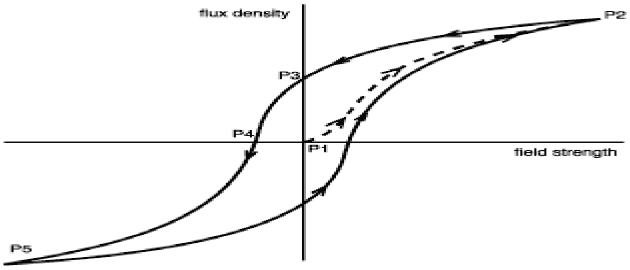

Fig. 13. Graphical representation of hysteresis.

E. Deadband

The sensor has a Deadband when angle phi is + 90 degrees and -90 degrees. This is because as shown in equation 1, the change in H-field becomes zero with these phi angles due to the inherent limitations of the boundary value problem in the mathematical model. Hence, the Deadband exist when angle phi is +90 and -90 degrees.

F. Output Range

The input is valid from r to infinity. It is valid at r due to boundary value conditions, and invalid within the Lorentz sphere due to the solutions obtained from the Laplacian.

The output ranges from Vref = 1.80V to Vmax = 12.4V. Vref is defined as the value when r = infinity. Vmax is defined as the value when r = R (boundary value condition).

G. Saturation

Using the values for our parameters from the output range section, Vref = 1.80V to Vmax = 12.4V.

H. Noise analysis

The noise of the whole sensor system originates predominantly from two sources: First, the noise from the magnetometer sensor from the background fluctuations in magnetic field strengths caused by electrical components and devices and the resistor thermal noise from the resistance in wires in the coils. Secondly, the noise from the interface circuit, such as thermal noise from the resistors, capacitors and the noise from the operational amplifier. Other sources of noise besides Johnson noise such as Shot noise and Flicker Noise are less significant.

All the thermal noise from resistors and capacitors can be given as:

Johnson noise calculations:

$$vR\_DEC = G_{DC}\sqrt{4k_bTR_{R1}\Delta f} = \sqrt{4(1.38\cdot 10^{-23}J/°K)(300°K)(0.6\Omega)1000Hz} = 3.1\eta V$$

$$vR\_SDC = G_{DC}\sqrt{4k_bTR_{R1}\Delta f} = \sqrt{4(1.38\cdot 10^{-23}J/°K)(300°K)(1.3\Omega)1000Hz} = 4.57\eta V$$

$$vR\_Amp1 = G_{DC}\sqrt{4k_bTR_{c1}\Delta f} = \sqrt{4(1.38\cdot 10^{-23}J/°K)(300°K)(82\Omega)1000Hz} = 36.3nV$$

$$vR\_Amp2 = G_{DC}\sqrt{4k_bTR_{c1}\Delta f} = \sqrt{4(1.38\cdot 10^{-23}J/°K)(300°K)(20000\Omega)1000Hz} = 560nV$$

$$\sigma_{total} \approx \sqrt{(3.1nV)^2(4.57\eta V)^2+(36.3\eta V)^2+(560nV)^2} = 0.56\mu V$$

Calculated resistance of wires in DEC = 0.6 Ohms. Calculated resistance of wires in SDC = 1.3 Ohms.

Using data provided from the Op-Amp data specification sheet, the summarized key values for the noise in the Op-Amp are:

Voltage Noise From Op-Amp RTI: e_{nv} = 3560nV
Current Noise From Op-Amp RTI (as a voltage): e_{ni} = 1.67nV
Resistor Noise RTI: e_{nr} = 4020nV
Total Noise RTI: $e_{n\ in}$ = √((3560nV)^2 + ((1.67nV)^2 + ((4020nV)^2) = 5369nV
Total Noise RTO: $e_{n\ out}$ = $e_{n\ in}$ * gain = (5369nV)(1) = 5369nV
Then, the total noise of the system and the Signal to Noise Ratio can be calculated as:

$$SystemNoise = \sigma_{system} = \sigma_{total} + \sigma_{other} \approx \sqrt{(\sigma_{total})^2 + (\sigma_{other})^2}$$

$$= \sqrt{(0.56\mu V)^2 + (5369nV)^2} = 5.40\mu V$$

$$SNR = 20\log\left(\frac{OutputSpan}{SystemNoise}\right) = 20\log\left(\frac{12.4-1.81}{5.40\mu V}\right)dB = 125dB$$

VII. Summary

The magnetometer and accompanying circuits have much potential for detecting perturbations in the Earth's magnetic field located up to 14cm for this proof of concept. The input and output ranges are reasonably measurable values with high enough resolution to handle the noise we considered in our analysis. The primary limitation of performance is the medium range of the magnetic field detection. Our measurement of interest falls off proportional to 1/r^3, and thus it is would additional specialized and sensitive instruments to accurately distinguish objects farther than 14cm away.

Future work for the sensor includes consideration of other noise sources in order to further improve its response to noise. In addition, sharper filters could be designed to better isolate the harmonics we are interested in analyzing. In order to improve on location mapping, a multi-sensor system would be necessary to triangulate the position of the perturbing source. This proof of concept shows that it is possible to construct vehicle sensors using magnetometers. Future research and developments into this area would provide methods of vehicle detection with work based on this current concept.

References

[1] http://www.ngdc.noaa.gov/geomag/
[2] http://www.nasa.gov/
[3] http://www.usgs.gov/
[4] http://www.ti.com/
[5] http://www.ozitronics.com/docs/k23.pdf
[6] http://datasheets.maxim-ic.com/en/ds/MAX1132-MAX1133.pdf
[7] http://www.analog.com/static/imported-files/data_sheets/AD637.pdf
[8] http://rfic.eecs.berkeley.edu/~niknejad/ee142_fa05lects/pdf/lect11.pdf
[9] http://epcos.com